Dispersion control of silicon nanophotonic waveguides using sub-wavelength grating metamaterials in near-and mid-IR wavelengths

Daniel Benedikovic, Mathias Berciano, Carlos Alonso-Ramos, Xavier Le Roux, Eric Cassan, Delphine Marris-Morini, Laurent Vivien

Research Article | Vol. 25, No. 16 | 7 Aug 2017 | OPTICS EXPRESS 19468

Optics EXPRESS

Dispersion control of silicon nanophotonic waveguides using sub-wavelength grating metamaterials in near- and mid-IR wavelengths

DANIEL BENEDIKOVIC,* MATHIAS BERCIANO, CARLOS ALONSO-RAMOS, XAVIER LE ROUX, ERIC CASSAN, DELPHINE MARRIS-MORINI, AND LAURENT VIVIEN

Centre de Nanosciences et de Nanotechnologies, CNRS, Universite Paris-Sud, Université Paris-Saclay, C2N – Orsay, 91405 Orsay cedex, France
**daniel.benedikovic@u-psud.fr*

Abstract: Controlling the group velocity dispersion of silicon nanophotonic waveguides has been recognized as a key ingredient to enhance the development of various on-chip optical applications. However, the strong wavelength dependence of the dispersion in waveguides implemented on the high index contrast silicon-on-insulator (SOI) platform substantially hinders their wideband operation, which in turn, limits their deployment. In this work, we exploit the potential of non-resonant sub-wavelength grating (SWG) nanostructures to perform a flexible and wideband control of dispersion in SOI waveguides. In particular, we demonstrated that the overall dispersion of the SWG-engineered metamaterial waveguides can be tailored across the transparency window of the SOI platform, keeping easy-to-handle single-etch step manufacturing. The SWG silicon waveguides overcladded by silicon nitride exhibit significant reduction of wavelength dependence of dispersion, yet providing intriguing and customizable synthesis of various attractive dispersion profiles. These include large normal up to low anomalous operation regimes, both of which could make a great promise for plethora of emerging applications in silicon photonics.

OCIS codes: (130.0130) Integrated optics; (050.6624) Subwavelength structures; (160.3918) Metamaterials; (260.2030) Dispersion; (230.7370) Waveguides; (040.6040) Silicon.

References and links

1. R. Soref, "The past, present, and future of silicon photonics," IEEE J. Sel. Top. Quantum Electron. **12**(6), 1678–1687 (2006).
2. A. Rickman, "The commercialization of silicon photonics," Nat. Photonics **8**(8), 579–582 (2014).
3. J. Leuthold, C. Koos, and W. Freude, "Nonlinear silicon photonics," Nat. Photonics **4**(8), 535–544 (2010).
4. M. A. Foster, A. C. Turner, J. E. Sharping, B. S. Schmidt, M. Lipson, and A. L. Gaeta, "Broad-band optical parametric gain on a silicon photonic chip," Nature **441**(7096), 960–963 (2006).
5. D. J. Moss, R. Morandotti, A. L. Gaeta, and M. Lipson, "New CMOS-compatible platforms based on silicon nitride and Hydex for nonlinear optics," Nat. Photonics **7**(8), 597–607 (2013).
6. Y. A. Vlasov, M. O'Boyle, H. F. Hamann, and S. J. McNab, "Active control of slow light on a chip with photonic crystal waveguides," Nature **438**(7064), 65–69 (2005).
7. R. M. Osgood, Jr., N. C. Panoiu, J. I. Dadap, X. Liu, X. Chen, I.-W. Hsieh, E. Dulkeith, W. M. J. Green, and Y. A. Vlasov, "Engineering nonlinearities in nanoscale optical systems: physics and applications in dispersion-engineered silicon nanophotonic wires," Adv. Opt. Photonics **1**(1), 162–235 (2009).
8. L. Zhang, A. M. Agarwal, L. C. Kimerling, and J. Michel, "Nonlinear Group IV photonics based on silicon and germanium: from near-infrared to mid-infrared," Nanophotonics **3**(4–5), 247–268 (2014).
9. J. Wang, R. Ashrafi, R. Adams, I. Glesk, I. Gasulla, J. Capmany, and L. R. Chen, "Subwavelength grating enabled on-chip ultra-compact optical true time delay line," Sci. Rep. **6**(1), 30235 (2016).
10. J. M. Chavez Boggio, D. Bodenmuller, T. Fremberg, R. Haynes, M. M. Roth, R. Eiserman, M. Lisker, L. Zimmermann, and M. Bohm, "Dispersion engineered silicon nitride waveguides by geometrical and refractive-index optimization," J. Opt. Soc. Am. B **31**(11), 2846–2857 (2014).
11. V. R. Almeida, Q. Xu, C. A. Barrios, and M. Lipson, "Guiding and confining light in void nanostructure," Opt. Lett. **29**(11), 1209–1211 (2004).

#295930 https://doi.org/10.1364/OE.25.019477
Journal © 2017 Received 12 May 2017; revised 22 Jul 2017; accepted 28 Jul 2017; published 3 Aug 2017

Optics EXPRESS

12. A. C. Turner, C. Manolatou, B. S. Schmidt, M. Lipson, M. A. Foster, J. E. Sharping, and A. L. Gaeta, "Tailored anomalous group-velocity dispersion in silicon channel waveguides," Opt. Express **14**(10), 4357–4362 (2006).
13. E. Dulkeith, F. Xia, L. Schares, W. M. Green, and Y. A. Vlasov, "Group index and group velocity dispersion in silicon-on-insulator photonic wires," Opt. Express **14**(9), 3853–3863 (2006).
14. L. Zhang, Y. Yue, R. G. Beausoleil, and A. E. Willner, "Flattened dispersion in silicon slot waveguides," Opt. Express **18**(19), 20529–20534 (2010).
15. L. Zhang, Q. Lin, Y. Yue, Y. Yan, R. G. Beausoleil, and A. E. Willner, "Silicon waveguide with four zero-dispersion wavelengths and its application in on-chip octave-spanning supercontinuum generation," Opt. Express **20**(2), 1685–1690 (2012).
16. M. Zhu, H. Liu, X. Li, N. Huang, Q. Sun, J. Wen, and Z. Wang, "Ultrabroadband flat dispersion tailoring of dual-slot silicon waveguides," Opt. Express **20**(14), 15899–15907 (2012).
17. X. Liu, W. M. J. Green, X. Chen, I.-W. Hsieh, J. I. Dadap, Y. A. Vlasov, and R. M. Osgood, Jr., "Conformal dielectric overlayers for engineering dispersion and effective nonlinearity of silicon nanophotonic wires," Opt. Lett. **33**(24), 2889–2891 (2008).
18. Y. Guo, Z. Jafari, A. M. Agarwal, L. C. Kimerling, G. Li, J. Michel, and L. Zhang, "Bilayer dispersion-flattened waveguides with four zero-dispersion wavelengths," Opt. Lett. **41**(21), 4939–4942 (2016).
19. H. Liang, Y. He, R. Luo, and Q. Lin, "Ultra-broadband dispersion engineering of nanophotonic waveguides," Opt. Express **24**(26), 29444–29451 (2016).
20. S. Serna, P. Colman, W. Zhang, X. Le Roux, C. Caer, L. Vivien, and E. Cassan, "Experimental GVD engineering in slow light slot photonic crystal waveguides," Sci. Rep. **6**(1), 26956 (2016).
21. R. Halir, P. Bock, P. Cheben, A. Ortega-Moñux, C. Alonso-Ramos, J. H. Schmid, J. Lapointe, D.-X. Xu, J. G. Wangüemert-Pérez, I. Molina-Fernández, and S. Janz, "Waveguide sub-wavelength structures: a review of principles and applications," Laser Photonics Rev. **9**(1), 25–49 (2015).
22. P. Cheben, D.-X. Xu, S. Janz, and A. Densmore, "Subwavelength waveguide grating for mode conversion and light coupling in integrated optics," Opt. Express **14**(11), 4695–4702 (2006).
23. P. J. Bock, P. Cheben, J. H. Schmid, J. Lapointe, A. Delâge, S. Janz, G. C. Aers, D.-X. Xu, A. Densmore, and T. J. Hall, "Subwavelength grating periodic structures in silicon-on-insulator: a new type of microphotonic waveguide," Opt. Express **18**(19), 20251–20262 (2010).
24. P. Cheben, P. J. Bock, J. H. Schmid, J. Lapointe, S. Janz, D.-X. Xu, A. Densmore, A. Delâge, B. Lamontagne, and T. J. Hall, "Refractive index engineering with subwavelength gratings for efficient microphotonic couplers and planar waveguide multiplexers," Opt. Lett. **35**(15), 2526–2528 (2010).
25. D. Benedikovic, P. Cheben, J. H. Schmid, D.-X. Xu, B. Lamontagne, S. Wang, J. Lapointe, R. Halir, A. Ortega-Moñux, S. Janz, and M. Dado, "Subwavelength index engineered surface grating coupler with sub-decibel efficiency for 220-nm silicon-on-insulator waveguides," Opt. Express **23**(17), 22628–22635 (2015).
26. P. Cheben, J. H. Schmid, S. Wang, D.-X. Xu, M. Vachon, S. Janz, J. Lapointe, Y. Painchaud, and M.-J. Picard, "Broadband polarization independent nanophotonic coupler for silicon waveguides with ultra-high efficiency," Opt. Express **23**(17), 22553–22563 (2015).
27. J. Gonzalo Wangüemert-Pérez, P. Cheben, A. Ortega-Moñux, C. Alonso-Ramos, D. Pérez-Galacho, R. Halir, I. Molina-Fernández, D.-X. Xu, and J. H. Schmid, "Evanescent field waveguide sensing with subwavelength grating structures in silicon-on-insulator," Opt. Lett. **39**(15), 4442–4445 (2014).
28. J. Flueckiger, S. Schmidt, V. Donzella, A. Sherwali, D. M. Ratner, L. Chrostowski, and K. C. Cheung, "Sub-wavelength grating for enhanced ring resonator biosensor," Opt. Express **24**(14), 15672–15686 (2016).
29. J. Wang, I. Glesk, and L. R. Chen, "Subwavelength grating filtering devices," Opt. Express **22**(13), 15335–15345 (2014).
30. D. Pérez-Galacho, C. Alonso-Ramos, F. Mazeas, X. Le Roux, D. Oser, W. Zhang, D. Marris-Morini, L. Labonté, S. Tanzilli, É. Cassan, and L. Vivien, "Optical pump-rejection filter based on silicon sub-wavelength engineered photonic structures," Opt. Lett. **42**(8), 1468–1471 (2017).
31. H. Yun, Y. Wang, F. Zhang, Z. Lu, S. Lin, L. Chrostowski, and N. A. F. Jaeger, "Broadband 2 × 2 adiabatic 3 dB coupler using silicon-on-insulator sub-wavelength grating waveguides," Opt. Lett. **41**(13), 3041–3044 (2016).
32. R. Halir, P. Cheben, J. M. Luque-González, J. D. Sarmiento-Merenguel, J. H. Schmid, G. Wangüemert-Pérez, D.-X. Xu, S. Wang, A. Ortega-Moñux, and I. Molina-Fernández, "Ultra-broadband nanophotonic beamsplitter using an anisotropic sub-wavelength metamaterial," Laser Photonics Rev. **10**(6), 1039–1046 (2016).
33. J. S. Penades, A. Ortega-Moñux, M. Nedeljkovic, J. G. Wangüemert-Pérez, R. Halir, A. Z. Khokhar, C. Alonso-Ramos, Z. Qu, I. Molina-Fernández, P. Cheben, and G. Z. Mashanovich, "Suspended silicon mid-infrared waveguide devices with subwavelength grating metamaterial cladding," Opt. Express **24**(20), 22908–22916 (2016).
34. Y. Wang, W. Shi, X. Wang, Z. Lu, M. Caverley, R. Bojko, L. Chrostowski, and N. A. F. Jaeger, "Design of broadband subwavelength grating couplers with low back reflection," Opt. Lett. **40**(20), 4647–4650 (2015).
35. J. Čtyroký, P. Kwiecien, and I. Richter, "Dispersion Properties of Subwavelength Grating SOI waveguides," *in Proceedings of Progress in Electromagnetic Research Symposium*, Stockholm, Sweden, Aug. 2013,1613–1617.
36. Z. Jafari and A. Zarifkar, "Fabrication-Friendly Subwavelength-Structure-Assisted Waveguide for Dispersion Engineering," Appl. Opt. **55**(32), 9084–9090 (2016).
37. Z. Jafari and A. Zarifkar, "Dispersion flattened single etch-step waveguide based on subwavelength grating," Opt. Commun. **393**, 219–223 (2017).

Optics EXPRESS

38. P. Kwiecien, I. Richter, and J. Čtyroký, "Comparison of 2D and 3D Fourier modal methods for modeling subwavelength-structured silicon waveguides," Proc. SPIE **8306**, 83060Y (2011).
39. B. Chmielak, M. Waldow, C. Matheisen, C. Ripperda, J. Bolten, T. Wahlbrink, M. Nagel, F. Merget, and H. Kurz, "Pockels effect based fully integrated, strained silicon electro-optic modulator," Opt. Express **19**(18), 17212–17219 (2011).
40. P. Damas, X. Le Roux, D. Le Bourdais, E. Cassan, D. Marris-Morini, N. Izard, T. Maroutian, P. Lecoeur, and L. Vivien, "Wavelength dependence of Pockels effect in strained silicon waveguides," Opt. Express **22**(18), 22095–22100 (2014).
41. D.-X. Xu, J. H. Schmid, G. T. Reed, G. Z. Mashanovich, D. J. Thomson, M. Nedeljkovic, X. Chen, D. V. Thourhout, S. Keyvaninia, and S. K. Selvaraja, "Silicon photonic integration platform: Have we found the sweet spot?" IEEE J. Sel. Top. Quantum Electron. **20**(4), 189–205 (2014).
42. G. Z. Mashanovich, F. Y. Gardes, D. J. Thomson, Y. Hu, K. Li, M. Nedeljkovic, J. Soler Penades, A. Z. Khokhar, C. J. Mitchell, S. Stankovic, R. Topley, A. A. Reynolds, Y. Wang, B. Troia, V. M. N. Passaro, C. G. Littlejohns, T. Dominguez-Bucio, P. R. Wilson, and G. T. Reed, "Silicon photonic waveguides and devices for Near- and Mid-IR applications," IEEE J. Sel. Top. Quantum Electron. **21**(4), 407–418 (2015).
43. S. Rytov, "Electromagnetic properties of a finely stratified medium," Sov. Phys. **2**, 466–475 (1956).
44. Lumerical Solutions, Inc., Available: *http://www.lumerical.com*.
45. L. Zavargo-Peche, A. Ortega-Moñux, J. G. Wangüemert-Pérez, and I. Molina-Fernández, "Fourier based combined techniques to design novel sub-wavelength optical integrated devices," Prog. Electromagnetics Res. **123**, 447–465 (2012).
46. K. Sakoda, *Optical properties of photonic crystals*, Vol. 80 (Springer Science & Business Media, 2004).
47. E. D. Palik, *Handbook of OpticalConstants of Solids*(Academic, 1998).
48. K. Luke, Y. Okawachi, M. R. E. Lamont, A. L. Gaeta, and M. Lipson, "Broadband mid-infrared frequency comb generation in a Si_3N_4 microresonator," Opt. Lett. **40**(21), 4823–4826 (2015).

1. Introduction

The silicon-on-insulator (SOI) has been established as a promising waveguide technology to realize key integrated nanophotonic components in various on-chip optical applications. The SOI offers inherent benefits such as nano-scale miniaturization, ultra-dense integration, as well as leveraging manufacturing processes that exist in microelectronics facilities [1,2].

The control of the dispersion in nanophotonic waveguides has been recognized as an essential ingredient to exploring a broad range of emerging linear and nonlinear optical applications [3–9], including parametric optical processes, frequency combs, or supercontinuum generation, to name a few. More recently, substantial research efforts have been put forward to engineering dispersion properties in a variety of structures and material platforms [3–20]. In a particular case of the dominant SOI platform, indeed, the dispersion can be readily controlled by adjusting cross-sectional dimensions of the waveguide [10–13], because of the high modal confinement offered by the high index contrast system. Apart from this straightforward approach, several different techniques have been explored, both theoretically and experimentally [14–20], allowing for variable dispersion engineering. This primarily includes the slot-assisted waveguide structure with horizontal and vertical geometries [14–16], conformal dielectric overlayers [17], multilayer guiding structures [18], double- and multi-cladded waveguides [19], or photonic crystal waveguides [20].

Sub-wavelength gratings (SWG), i.e. nanophotonic segmented structures with dimensions on a scale below the wavelength of light, have enabled a profound technological concept of local refractive index engineering [21]. Since, the first demonstrations of an optical waveguide with a SWG metamaterial core by Cheben et al. [22–24], metamaterial SWG waveguides have attracted a strong research interest, because of their great potential for customizing light propagation properties in planar waveguides [21]. More recently, applications include, but not limited to, efficient optical coupling interfaces [25,26], bio-sensing devices [27,28], optical filters [29,30], broadband directional [31] and multimode interference couplers [32], or suspended Si waveguides for extended mid-infrared (mid-IR) operation [33]. Expanding the spirit of refractive index engineering into a broader sense, SWG metamaterials are poised to locally synthesize different group indices, thereby enabling additional flexibility to control the overall waveguide dispersion. Recently, several broadband metamaterial engineered photonic devices have been reported [26,31,32,34], showing albeit an indirect route of dispersion engineering. From a fundamental point of view, it is practically

Optics EXPRESS

more attractive to explore dispersion properties of such metamaterial waveguides, since they hold the promise of forming basic building blocks for complex nanophotonic components [35–38]. So far, the SWG metamaterials have only been partially examined, merely to assist the dispersion controlling in silicon waveguide, exploiting the well-known mode transition effect [36,37]. However, the intrinsic dispersion characteristics of conventional strip SWG waveguides remained unexplored.

In this work, we exploit the potential of SWG metamaterials for the development of flexible and wideband dispersion control in the silicon waveguides overcladded by silicon nitride layer. In particular, we showed that the overall dispersion of SWG-based metamaterial waveguides can be a useful design strategy to substantially relax the typical strong wavelength dependence of conventional silicon waveguides. This way, the dispersion of the metamaterial-controlled silicon waveguide can be tuned in a wide spectral range, yet keeping single-etch step fabrication. The advantageous utilization of SWG nano-structuration enables profound design capability for synthesizing various attractive dispersion profiles, ranging from large normal up to low anomalous operation regimes. Those dispersion characteristics of silicon waveguides engineered by SWG segmentation could be of great interest for broad application scenarios in silicon photonics.

2. Design and simulation methodology

2.1 Fundamental design considerations

In this work, the silicon nitride (Si_3N_4) is utilized as an upper cladding material (superstrate). The appropriate choice of the cladding is a critical design consideration, particularly relevant in case of waveguide dispersion engineering. This choice solely dictates the overall wavelength dependence of the nanophotonic guiding system [8]. More specifically, for conventional waveguides built on inherently high index contrast Si platform [with a cross-section shown in Fig. 1(a)], the overall waveguide dispersion typically exhibits strong wavelength-dependent behavior, as shown in Fig. 1(b). Here, a typical single-mode strip Si waveguide of 220-nm in thickness and 500-nm in width is considered, with different upper cladding materials (air, silicon dioxide (SiO_2), and Si_3N_4). In the case of air or SiO_2 claddings, the large index difference between the waveguide core and the respective cladding is responsible for the comparatively higher waveguide dispersion, which hinders the development of wideband optical applications. The Si_3N_4 as a cladding material still enables index contrast that is sufficiently high to allow for waveguide dispersion engineering, while significantly mitigates the wavelength dependence of dispersion, i.e. the wavelength-dependent profile of waveguide dispersion becomes virtually flat compared to the typically used claddings (air or SiO_2). Albeit, beyond the scope of this work, it is worth highlighting that the advantageous combination of Si and Si_3N_4 could pave a way for extending on-chip functionalities in photonic applications. More specifically: (i) Unlike Si, Si_3N_4, has a large bandgap, thereby does not suffer from the undesired nonlinear losses caused by two-photon absorption across the near-infrared (near-IR) spectral region [5]; (ii) Si has no natural second-order nonlinearities, thereby suffers from the inherent lack of high-speed electro-optic effect [3,5], while the utilization of Si_3N_4 as a cladding on top of Si waveguides facilitates the development of strain-induced nonlinearities for ultra-fast optical modulation [39,40]; (iii) The cubic nonlinear effects are typically available in both materials [3,5], and both are comparatively larger than that of pure silica [8]; (iv) Both Si and Si_3N_4 materials are well-established for a wide range of passive and active photonic devices, indeed, with a mature CMOS-compatible fabrication [1–3,5].

The two-dimensional (2-D) schematic of vertical geometry of the sub-wavelength grating (SWG) metamaterial waveguide is shown in Fig. 1(c). The guiding structure comprises composite waveguide core of thickness H_c and width W_c. This is formed by the non-resonant nanophotonic structure, here implemented as a longitudinally-invariant periodic array (along the z-direction) of fully etched rectangular trenches of length L_t filled by the lower refractive

Optics EXPRESS

index material separated by unetched silicon (Si) blocks, with a length L_b. The lengthwise period of SWG array, defined as $\Lambda = L_b + L_t$, is smaller than half of the effective wavelength in a metamaterial waveguide, thereby mitigating losses and wavelength resonances by frustrating the diffraction [21]. The duty cycle of the SWG structure is denoted as $DC = L_b/\Lambda$.

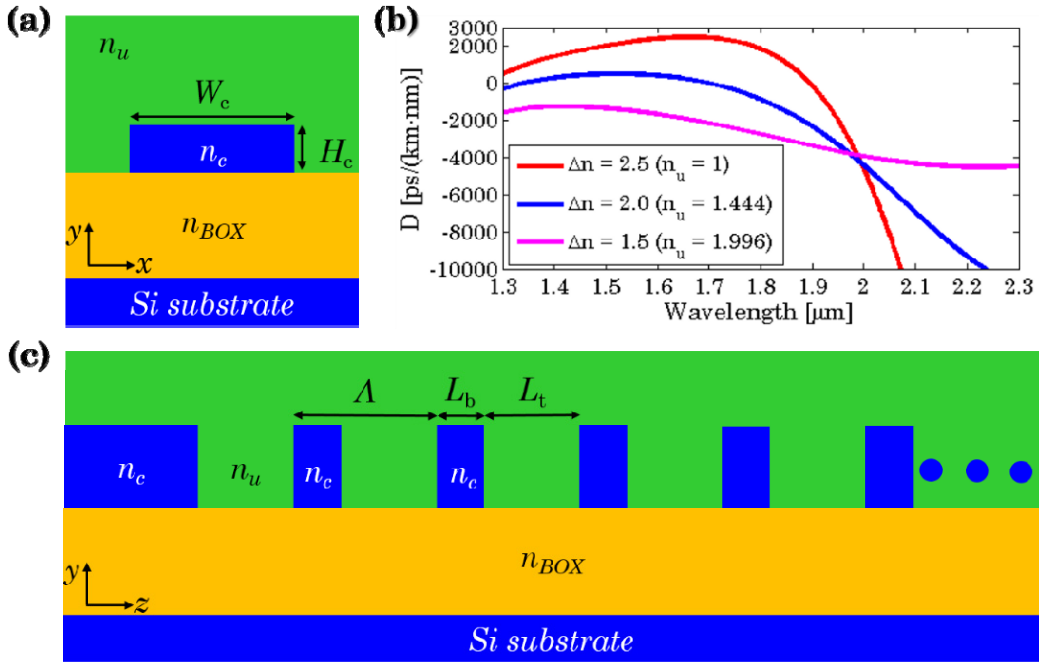

Fig. 1. (a) Two-dimensional (2-D) cross-sectional view (*x*-*y* plane) of conventional Si strip waveguide. (b) The evolution of the waveguide dispersion as a function of wavelength for a single-mode Si strip waveguide, with different upper claddings: air (n_u = 1), SiO_2 (n_u = 1.444), and Si_3N_4 (n_u = 1.996). The waveguide core dimensions were: 220-nm of thickness and 500-nm of width, respectively. (c) 2-D vertical view (*y*-*z* plane) of a SWG waveguide.

Our investigations were performed for the transverse electrical (TE) polarization and operation in a wavelength range from 1.3 μm to 3.7 μm. To completely exploit the transparency window of SOI, waveguide dispersion designs have been carried out on various silicon thicknesses. The 220-nm- and 300-nm-thick SOI wafers are typically used by academia and industry for the development of silicon photonics devices [41], while 400-nm- and 500-nm-thick Si waveguides are desirable for emerging applications in the mid-IR wavelengths [42].

2.2 Simulation strategy

In order to estimate the dispersion trends in SWG metamaterial waveguides, at a first stage, it is necessary to calculate the effective index of waveguides. In the SWG waveguide, the electromagnetic field propagates in the form of Bloch-Floquet modes, which are theoretically lossless [21]. The propagation of Bloch-Floquet modes is restricted by two factors. First, the effective index n_{BF} of the fundamental mode has to meet the following condition: n_{SiO2} or $n_{Si3N4} < n_{BF} < \lambda/(2\Lambda)$. The left-sided limit ($n_{SiO2}$ or $n_{Si3N4} < n_{BF}$) assures that the optical field confinement is sufficiently high to guide a mode inside the metamaterial waveguide core, while the upper limit ($n_{BF} < \lambda/(2\Lambda)$) avoids the formation of Bragg reflection zones. To calculate the effective index of the fundamental TE-polarized Bloch-Floquet mode, different simulation strategies were considered:

Optics EXPRESS

(1) Effective Medium Theory and 3-D homogeneous equivalent waveguide simulations: For most practical cases of interest, the longitudinally periodic structure operates in the SWG regime, i.e. the operation regime, in which the SWG period (Λ) is small enough compared to the designed wavelength (λ) [21]. Here, the inherent behavior of the SWG waveguide may be treated as an optically equivalent waveguide of metamaterial refractive index. This refractive index depends on the grating geometry, polarization, constituent materials, and wavelength. This metamaterial refractive index is estimated by means of Effective Medium Theory (EMT) [43]. The optically equivalent waveguide is described as the conventional strip waveguide of homogeneous metamaterial core that has the same transversal cross-section (thickness and width). Then, the Bloch-Floquet effective index of the SWG waveguide is approximated by the effective index of the fundamental mode in the homogeneous equivalent waveguide. Simulations were performed by full-vectorial three-dimensional (3-D) Finite Difference Eigenmode (FDE) solver [44]. The Perfect Matched Layers (PMLs) were used as boundary conditions. The uniform mesh grid size of 15 nm was used in simulations.

(2) Effective Index Method and 2-D Bloch-Floquet simulations: The 3-D problem was firstly transformed to the equivalent 2-D problem with the help of the Effective Index Method [38]. Here, the geometrical variations in the transversal cross-section of the waveguide were taken into the account, which in turn, yielded changes in the effective mode index. The calculated effective index is sub-sequently used for the final 2-D longitudinally periodic waveguide and the complex Bloch-Floquet modal analysis was carried out. This was performed by semi-rigorous 2-D Fourier-type simulation tool based on the Eigenmode Expansion Method (F-EEM) [45], optimized for analyzing the periodic waveguides.

(3) The rigorous full-vectorial 3-D Finite Difference Time Domain (FDTD) simulations: The FDTD Solutions tool [44] was also used for further study. Here, the real 3-D structure of the SWG waveguide was considered. Taking the benefit of the structure periodicity (the SWG waveguide is periodic along the propagation direction), the 3-D structure was simulated along one period, where Bloch boundary conditions were applied. This simulation strategy follows bandstructure calculations used in photonic crystals [46]. For the rest, the PMLs were used as boundary conditions. The simulation grid size was: $\Delta x/\Delta y/\Delta z$ = 10 nm/10 nm/10 nm. For Bloch-Floquet mode excitation, randomly distributed dipoles were used as an input source. From the recorded time signals, the resonant Bloch-Floquet modes were determined with the help of Fourier Transform (FT).

It is worth nothing that in afore-described approaches, the intrinsic dispersion of constituent materials (Si, SiO_2, and Si_3N_4) was taken into the account via Sellmeier equations [47,48]. The dispersion characteristics of SWG metamaterial waveguides were calculated using the formula for dispersion parameter D, expressed in [ps/(km·nm)]: $(-\lambda/c)\cdot(d^2 n_{BF}/\lambda^2)$.

Optics EXPRESS

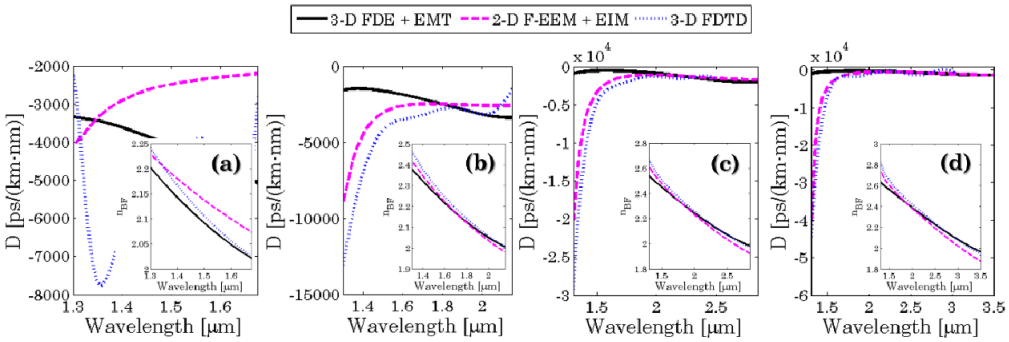

Fig. 2. Comparison of different simulation strategies for dispersion of the SWG metamaterial waveguides. For simulations, following transversal geometries were considered: (a) H_c = 220 nm and W_c = 500 nm; (b) H_c = 300 nm and W_c = 600 nm; (c) H_c = 400 nm and W_c = 800 nm; and (d) H_c = 500 nm and W_c = 1000 nm. The longitudinal dimensions of the SWG waveguide were: the period Λ = 200 nm and the duty cycle DC = 50%. Insets: Spectral evolution of the calculated fundamental Bloch-Floquet modes for various SWG metamaterial waveguides.

Simulation results obtained with different strategies are shown in Figs. 2(a) – 2(d), illustrating the spectral evolution of the waveguide dispersion and the evolution of calculated indices of fundamental Bloch-Floquet modes [insets of Figs. 2]. For this comparative study, following waveguide dimensions were considered: (a) H_c = 220 nm and W_c = 500 nm; (b) H_c = 300 nm and W_c = 600 nm; (c) H_c = 400 nm and W_c = 800 nm; and (d) H_c = 500 nm and W_c = 1000 nm. For the longitudinal waveguide geometry, we used SWG period Λ = 200 nm, with a duty cycle DC = 50%. To this end, from the performed simulations, several important conclusions may be drawn:

(i) Generally, it is not possible to accurately estimate the trends of the waveguide dispersion in case of sub-micrometric Si waveguides that are engineered by SWG structuration [see Fig. 2(a) and 2(b), black curves] only by using analytical EMT approximations. On the other hand, the 3-D FDE + EMT simulation approach seems to be suitable merely for Si waveguide that have larger cross-sectional areas [see Figs. 2(c) and 2(d)], however, only for longer wavelength. The intrinsic resonant effect of SWG structures, operating close to the Bragg limit at shorter wavelengths, is completely hidden within this approach.

(ii) For SWG metamaterial waveguides with a larger cross-sectional area [see Figs. 2(b), 2(c) and 2(d)], the semi-rigorous 2-D F-EEM + EIM calculations are in very good agreement with the rigorous, although computationally demanding, 3-D FDTD calculations. Indeed, both simulation strategies advantageously take into the consideration the natural resonant/non-resonant behavior of SWG structures. This way, the semi-rigorous 2-D F-EEM approach appears to be a feasible design strategy to estimate the overall trends of dispersion, especially in terms of simulation complexity and computational time.

3. Results and discussion

The potential of the SWG nano-structuration to control the overall dispersion of Si waveguides is shown in Figs. 3(a) - 3(c), respectively. Firstly, different thicknesses of Si waveguides were considered, with a typical transversal aspect ratio of ~1:2. This results in waveguide cross-sections of H_c = 300 nm by W_c = 600 nm; H_c = 400 nm by W_c = 800 nm; and H_c = 500 nm by W_c = 1000 nm, respectively. For these cross-sectional dimensions, both conventional strip Si and metamaterial waveguides are designed to preserve single-mode operation [13,41]. This is generally a superior propagation scenario in order to avoid potential modal cross-talk. However, in practical dispersion-engineered waveguides [5,8], this preferential single-mode condition can be considerably relaxed in order to afford substantial enhancement of the dispersion bandwidth. The longitudinal dimensions of the sub-

Optics EXPRESS

wavelength grating are: Λ = 200 nm, which is small enough to suppress diffraction over the spectral range under investigation, and different lengths of Si segments, i.e. duty cycles of *DC* = 25%; *DC* = 50%; and *DC* = 75%.

For shorter wavelengths of the SOI transparency window, the fundamental mode propagating through the waveguide is typically well-confined inside the composite core of the metamaterial waveguide, thereby waveguide dispersion profiles are mostly governed by the longitudinal geometry of the sub-wavelength nanostructure. Generally, by increasing the duty cycle, i.e. increasing the amount of Si within the SWG period, which in turn, enhances the vertical index contrast between the metamaterial waveguide core and Si_3N_4 cladding, the modal confinement of the SWG metamaterial waveguide increases as well. More importantly, at shorter wavelengths, the waveguide operates on the edge of the Bragg reflection zone (n_{Bragg} of ~3.25, for Λ = 200 nm at 1.3 μm), thus characteristics of the effective mode index are inherently more affected by the geometry of the sub-wavelength grating.

The trends of the overall dispersion in SWG metamaterial waveguides are more pronounced, once we provide a comprehensive comparison of the calculated dispersion profiles in respect to the waveguide thickness, as shown in Fig. 3, for the particular longitudinal geometry of the SWG nanostructure. Generally, for a fixed SWG geometry, it is apparent that the metamaterial waveguides become less dispersive for thicker Si layers, originating from the improved vertical optical confinement. As a result, the increase in the Si waveguide thickness produces a direct vertical upshift of the dispersion profile. The absolute values of the waveguide dispersion were smaller, gradually approaching zero dispersion regions up to the ultra-low anomalous (positive) dispersion regime, as shown in the insets of Figs. 3(b) and 3(c), respectively.

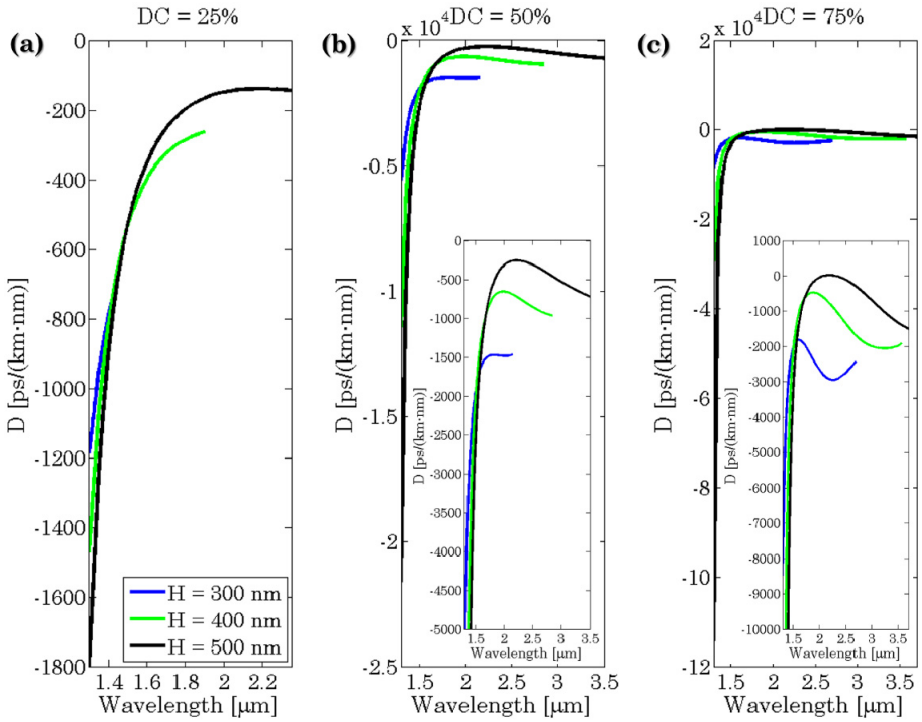

Fig. 3. Comparison of the dispersion as a function of wavelength for various transversal geometries of silicon waveguides, with an aspect ratio of 1:2 (thickness to width ratio) and different duty cycles of the SWG structure. (a) *DC* = 25%; (b) *DC* = 50%; and (c) *DC* = 75%. Insets of (b) and (c): Detailed views on calculated spectral dispersion profile.

Optics EXPRESS

In all cases illustrated in Fig. 3, it can be observed that for shorter wavelengths, the SWG metamaterial waveguides exhibited ultra-large normal dispersion characteristics. Since, for thicker Si waveguide, the effective index of the Bloch-Floquet mode proportionally increases, the effect of normal dispersion is even stronger in that case. The absolute values of dispersion are comparatively higher at shorter wavelengths and for larger lengths of Si segments. The combined interplay and collective contribution of: (i) the SWG geometry, operating close to the Bragg reflection zone; (ii) increased vertical confinement of the Si layer; and (iii) strong material dispersion of Si close to the material bandgap, results in the obtained ultra-strong normal dispersion profiles. Meanwhile, the normal dispersion operation regime could be useful for the realization of integrated photonic components for on-chip pulse compression or development of optical delay lines.

On the other hand, with the increase in wavelength, in general, by increasing the wavelength-to-period ratio, in particular, one can observe very sharp increase of the dispersion curves. In this spectral region, the effective mode index (for fixed transversal and longitudinal geometry) becomes more delocalized from the waveguide core and its optical properties are comparatively more affected by the optical properties of Si_3N_4 segments instead of the Si properties. Far away from the Bragg zone, i.e. the SWG metamaterial waveguide operates in true SWG regime, it can be seen that dispersion profiles are virtually flat over the wide spectral range. The sub-wavelength grating waveguide acts as an optically equivalent homogenous metamaterial, whose propagation properties are driven by the spatial averaging effect. This clearly demonstrates that the SWG nano-structuration of the Si waveguides holds the great promise for controlling the overall dispersion characteristics, particularly in term of their absolute values as well as in term of their spectral profile, thereby substantially alleviating the strong wavelength dependence of the waveguide dispersion.

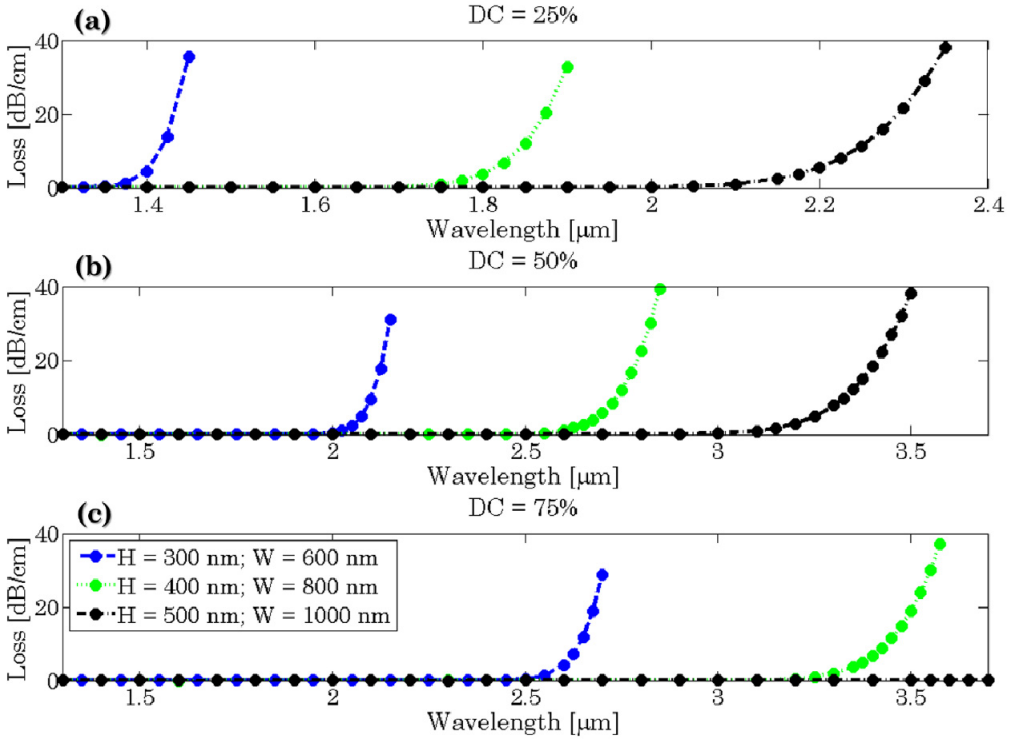

Fig. 4. Comparison of waveguide losses as a function of wavelength for various transversal geometries of SWG waveguides, with an aspect ratio of 1:2 (thickness to width ratio) and different duty cycles of the SWG structure. (a) *DC* = 25%; (b) *DC* = 50%; (c) *DC* = 75%.

Optics EXPRESS

Furthermore, for developing feasible photonic waveguides and complex components with engineered dispersion, waveguide losses play a critical role. This is particularly important for SWG-structured metamaterial waveguides, since propagation properties of such waveguides depend on the waveguide geometry comparatively more than in case of conventional Si waveguides. For dispersion controlling, the modal confinement is of essential interest, since it is directly related to both propagation properties such as waveguide losses and effective mode index, respectively. To estimate the loss evolution in SWG waveguides, the 3-D full-vectorial analysis was performed [44]. In Figs. 4(a) - 4(c) is shown the spectral evolution of losses of investigated SWG metamaterial waveguides, considering different cross-sectional and longitudinal geometries. From the performed simulations, it becomes apparent that for smaller duty cycle (larger gap of grating trenches with lower refractive index material, [see Fig. 4(a)]), SWG metamaterial waveguides experience more losses due to the reduced confinement of the optical field, i.e. the optical field is more delocalized from the waveguide core. The modal confinement dramatically diminishes with the increasing wavelength, thereby making the space for losses. This way, the useful transparency window of the guiding structure is substantially limited. Conversely, as shown in Figs. 4(b) and 4(c), for larger duty cycles (smaller gaps of grating trenches), the mode delocalization effect decreases (more high refractive index material within the SWG period), which in turn, extends the transparency window of the guiding structure. As predicted by simulations, while the optical field confinement is optimal, the waveguide losses may be considered to be negligible. This confirms the theoretically lossless propagation of the fundamental Bloch-Floquet modes. Furthermore, it is interesting to follow that for SWG waveguides of fixed duty cycle and of thinner waveguide core, the sharp increase of waveguide losses can be observed. This is particularly caused by the fact that with increasing wavelength, by natural behavior, the effective index of the Bloch-Floquet mode gradually approaches the material index of the superstrate (Si_3N_4). This effect is more pronounced (the rate of this approach) in case of thinner waveguides, because the proper optical confinement is rapidly lost. Therefore, beyond the cut-off wavelengths, the mode is no longer guided inside the metamaterial waveguide core and it will radiate into the upper cladding, yielding significant contribution to losses.

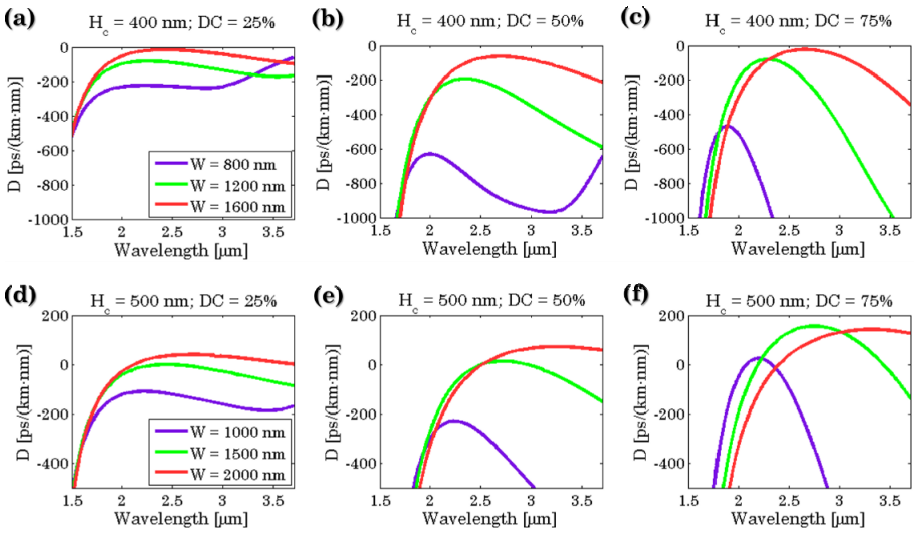

Fig. 5. The evolution of the dispersion as a function of wavelength for a SWG metamaterial waveguide with a thickness of 400-nm and 500-nm, considering different aspect ratios and various duty cycles. (a) H_c = 400 nm and DC = 25%; (b) H_c = 400 nm and DC = 50%; (c) H_c = 400 nm and DC = 75%; (d) H_c = 500 nm and DC = 25%; (e) H_c = 500 nm and DC = 50%; and (f) H_c = 500 nm and DC = 75%.

Optics EXPRESS

In Fig. 5, it is shown the evolution of the dispersion as a function of the wavelength for different transversal and longitudinal geometries of the SWG metamaterial waveguides. Here, various transversal aspect ratios of 1:2; 1:3; and 1:4 are considered, with a fixed waveguide thicknesses of 400-nm [Figs. 5(a) - 5(c)] and 500-nm [Figs. 5(d) - 5(f)], respectively. The duty cycles were: *DC* = 25%; *DC* = 50%; and *DC* = 75%. Generally, for larger Si waveguide widths and fixed Si waveguide thickness, it can be observed that spectral curves of the overall dispersion are red-shifted, i.e. the peak values of the absolute dispersion are moved towards longer wavelengths. Furthermore, for a fixed longitudinal geometry of the SWG structure, the increase in the transversal aspect ratio of the Si waveguide affords enhancement in the absolute value of the waveguide dispersion. In other words, this pushes the spectral dispersion profile from the normal dispersion regime towards the anomalous regime. In addition, the increase of the transversal aspect ratio yields at the same time the substantial enlargement of the spectral bandwidth of the respective dispersion profile. This way, the cut-off wavelengths are moved towards the longer wavelengths, i.e. hindering the mode radiation towards the superstrate and facilitating the exploitation of the full SOI transparency window. It is interesting to follow that this way, the SWG waveguide affords a useful ultra-wideband dispersion control. It can be seen in Figs. 5(a) - 5(c) that the calculated dispersion profiles are virtually flat in wide wavelength range, with an ultra-low or a moderate normal dispersion. This spectral dispersion features would be desirableto implement photonic functionalities for linear broadband dispersion compensation in optical communications, Kerr-type combs generation, or optical pulse shaping. On the other hand, in case of 500-nm-thick Si waveguide and *DC* = 75% [see Fig. 5(f)], the dispersion reaches the peak of 24 ps/(km·nm) at 2.20 μm, with an anomalous dispersion bandwidth of ~250 nm, for a transversal aspect ratio of 1:2. For an aspect ratio of 1:3, the peak value of dispersion is 156 ps/(km·nm) at 2.75 μm, with an extraordinary 1240-nm-wide dispersion bandwidth. Compared to case of 1:2 aspect ratio, this yields a five-hold enhancement of the anomalous dispersion bandwidth. In case of 1:4 aspect ratio, the peak dispersion is 142 ps/(km·nm) at a wavelength of 3.3 μm and the bandwidth is theoretically larger than 1300-nm, since 3.7-μm in wavelength is the edge of the SOI transparency [42]. These attributes make the SWG metamaterial waveguides particularly attractive choice in nonlinear photonic applications, demanding appropriate controlling of the phase-matched processes across wide spectral bandwidths such as supercontinuum and frequency comb generations or parametric conversions.

4. Conclusions

In summary, we report on waveguide dispersion designs by exploiting the profound technological concept of the SWG nano-patterning implemented in a dominant silicon-on-insulator platform. Specifically, we demonstrated that the overall dispersion of SWG metamaterial waveguides can be seamlessly engineered, allowing flexible and wideband dispersion control across the transparency window of the silicon-on-insulator platform, while keeping simplicity in the waveguide fabrication. The advantageous utilization of Si and Si_3N_4 segments interlaced on a scale bellow the wavelength of light alleviates the strong wavelength dependence of conventional Si waveguides. We showed that the SWG structures enable customizable synthesis of different attractive dispersion profiles, ranging from ultra-large normal up to low anomalous operation regimes. The SWG metamaterial waveguides hold immense promise for broad nanophotonic application scenarios, particularly interesting for the development of complex photonic components with extended functionality for optical communications, dispersion compensation, and optical signal processing.

Funding

European Research Council (ERC) under the European Union's Horizon 2020 Research and Innovation Program (ERC POPSTAR - grant agreement No 647342).